

Multiscale monsoon variability during the last two climatic cycles revealed by spectral signals in Chinese loess and speleothem records

Y. Li¹, N. Su^{2,3}, L. Liang¹, L. Ma¹, Y. Yan¹, and Y. Sun¹

¹State Key Laboratory of Loess and Quaternary Geology, Institute of Earth Environment, Chinese Academy of Sciences, Xi'an, Shaanxi 710061, China

²College of Science, Technology and Engineering, James Cook University, Cairns, Queensland 4870, Australia

³School of Mathematics and System Science, Shenyang Normal University, Shenyang, Liaoning 110034, China

Correspondence to: Y. Li (liying@ieccas.cn)

Cpd-2014-135-referee-report-1

1. First, in ABSTRACT, the last sentence says the same conclusion as that in Sun et al's paper (Nature Geo, 2012). If that is the case, the section 4.2 is improper. I suggest that authors should discuss a possible link of millennial and orbital changes of the winter and summer monsoons, if possible, discuss why components of the millennial-scale changes are so minor in both the summer and winter monsoon records.

Reply: We agree that the conclusion drew from section 4.2 is parallel with that in [Sun et al., 2012](#), but extended the millennial winter monsoon oscillation back to the last two glacial cycles. Sun et al. matched 60-kyr raw particle grain size and speleothem $\delta^{18}\text{O}$ series and found reconstructed millennial-scale variations are broadly correlated, suggesting a common driving force between East Asian winter and summer monsoon. In this manuscript, the raw 260-kyr grain size and speleothem $\delta^{18}\text{O}$ records are firstly decomposed by the approach of EMD, and only components on millennial scale are combined and correlated. Our results show that the similar rapid changes between East Asian winter and summer monsoon are not only evident during the last glaciation, but also persistent during the last two glacial cycles. We clarified these differences in section 4.2 (see lines 21-24, 27-28, page 9, and lines1-5, page 10).

The suggestion about plausible linkage between winter and summer monsoon signals on various timescales and the minor millennial-scale contribution are very interesting. Since the implication of speleothem $\delta^{18}\text{O}$ on summer monsoon intensity remains controversial, particularly the orbital-scale variability, we may consider the issues in the future based on high resolution proxy indicators of summer and winter monsoon derived from the same loess sequence.

2. Second, deleting some descriptions of analytical procedures and field work in Section 2

and in the acknowledgements, because all of the grain size data have been already published elsewhere.

Reply: We have already deleted the sample pretreatment in section 2 and some people in the acknowledgements.

3. Third, clarifying a relationship of the four papers in INTRODUCTION: a paper in Catena (2011), Sun et al (2012), Sun et al (2015) and this manuscript. I know what different things in the four papers, but readers do not.

Reply: The [Catena paper](#) is regarding the scanning XRF evaluation of loess U-channel samples from Gulang section, and has no relation with this work. The composed grain size data of Gulang section were originally submitted to *Climate of the Past* last October, about one month earlier than the paper submitted to *QSR*. Due to the quick reviewing and acceptance of the paper to *QSR*, we have to clarify that the grain size data and chronology in this manuscript were adopted from the published *QSR* paper. The major difference between this work and earlier paper in 2012 and 2015 has been clearly stated in the section of Data and Method (see lines 7-9, page 4).

Cpd-2014-135-referee-report-2

1. The $\delta^{13}\text{C}$ record of the Gulang section has similar time resolution as the grain size record. Thus, why don't they replace stalagmite $\delta^{18}\text{C}$ with the $\delta^{13}\text{C}$ of the Gulang loess sequence to perform the same mathematical analyses? They should depend on their own records which are from the same sequence under the same environmental background rather than the cave records in a totally different environment. This might be more convincing.

Reply: Thank you for this suggestion. We do not use $\delta^{13}\text{C}$ of the Gulang loess sequence as a summer monsoon index in this study for two reasons. Firstly, there is resolution difference between $\delta^{13}\text{C}$ (10-cm interval) and grain size (2-cm interval) records of Gulang section. The

10-cm resolution is not good enough to address millennial monsoon variability, and we are trying to conduct much higher resolution of the $\delta^{13}\text{C}$ analyses. Secondly, Gulang $\delta^{13}\text{C}$ record had not fully been constructed when we submitted this manuscript last October, though it's now published due to a swift reviewing process. If we employ Gulang $\delta^{13}\text{C}$ record to replace speleothem $\delta^{18}\text{O}$ record at this stage, we need to do quite a lot work in terms of data processing and manuscript revision and may wait for another long period for review process. Anyhow, we will address the orbital and millennial variability of both winter and summer monsoon in the future using much higher and longer records from Chinese loess.

Cpd-2014-135-referee-report-3

1. In order that the readers could reproduce the results, I ask the authors to consider the following requests:

- Provide the grain size data in a file, and explain how you made the connection between the two sections (the upper 20m one and the 50m one). Details about the dating procedure must be provided as well, i.e. the details about the matching with CHILOMOS.

- To what I have seen in the reference (Wang, 2008, Nature) given by the authors, the speleothem $d18\text{O}$ record from Sanbao/Hulu cave is not a unique time series but it is rather composed multiple fragments. Please explain the procedure to get the time series presented on figure 2. I also ask the authors to provide the data of the full record, presented on figure 2, in a supplementary file.

- Please provide in a supplementary material all the input parameters used for REDFIT, MTM and EMD. If the data were interpolated before MTM, please specify the kind of interpolation as well as the time step. Think that the reader must be able to reproduce figures 3, 4 and 5.

Reply: a. The grain size data in this manuscript covers a episode of time span of the data employed in [Sun et al., 2015](#); the latter series has already been published although it is submitted later than this manuscript. In this revision version, we used the published data directly. We will certainly upload the grain size data as a supplement. Chronologies of our

grain size time series and CHILOMOS have already been detailed in [Sun et al \(2015\)](#) and [Yang and Ding \(2014\)](#), respectively. In this study, we only try to match two grain size time series without any further tuning as shown in figure 2.

b. We clarified how we construct the speleothem $\delta^{18}\text{O}$ record in lines 10-14, page 4. The detail information about how to combine different stalagmites together can be found in Figure 1 in [Wang et al., 2008](#) and Figure 2 in [Cheng et al., 2009](#) for the period of 0-224 kyr and 224-260 kyr, respectively. The $\delta^{18}\text{O}$ data of each stalagmite has already been provided in supplementary files of the above two papers. We will provide the data of the full speleothem $\delta^{18}\text{O}$ record used in this study.

c. Before MTM, we interpolated the raw grain size and speleothem $\delta^{18}\text{O}$ data using linear interpolation approach by 100 yr. We will provide the input parameters of REDFIT and MTM, and the code of EMD.

2. Using both the Lomb-Scargle and MTM tools to perform spectral analysis is a very good choice, but the differences between REDFIT and MTM should be better explained.

Reply: In lines 2-9, page 5, we added more description about both advantages and disadvantages of MTM and REDFIT programs. Similar periodicities were detected using these two approaches for both loess and speleothem records (Figure 3), confirming the reliability of the spectral results in this manuscript.

3. page 6 row 7: « significance test which is not proportional to the power of spectrum » . I don't understand. Isn't it the case with REDFIT as well?

Reply: We have already deleted that sentence.

4. About the Empirical Mode decomposition:

- Please provide the reference for the code you used (reference « Huang et al. 1998 » is not sufficient since it does not provide any code), or provide your code as supplementary material.

- at row 19: « avoiding arbitrariness in the choices of frequency bands ». How does it work?
How are determined the 6 frequency bands on figure 4?

Reply: a. We firstly downloaded and installed the EMD toolkit on the MATLAB, then we wrote the code based on the EMD decomposing procedure. We will provide the code as a supplementary material.

b. Unlike filtering approach where frequency bands are beforehand settled, EMD iteratively decomposes the raw complex signal into a series of elementary intrinsic model function (IMF) components, and thus artificial choices of frequency bands can be avoided. After the generation of IMFs, we did spectral analysis on each IMF and got the spectral results in Figure 4 and 5.

5. Legend for figure 2: What is OSL dating? If a correlation with the Lisiecki and Raymo stack were performed, it should be explained in the main text, together with the dating procedure. The same remark holds for « OSL » dating

Reply: OSL dating is optically stimulated luminescence dating, the legend of Figure 2 has already been revised. In line 29, page 3 and lines 1-4, page 4, we emphasized that the grain size data employed in this manuscript were from [Sun et al., 2012](#) and [Sun et al., 2015](#), and the chronology were constructed based on [Sun et al., 2015](#). The selection of OSL ages for the upper 20 m and tie points linking rapid changes in mean grain size with the boundaries of marine isotope stages (MIS) recorded by the benthic $\delta^{18}\text{O}$ record for the lower 50 m can be fully found in Figure 2 in [Sun et al., 2015](#).

6. Figure 3: Start the frequency scale at $1/[\text{length of the time series}]$, i.e. At approximately 0.004 kyr^{-1} .

Reply: We have amended the tick range of x-coordinate in Figure 3, starting from 0.004 cycles/kyr.

7. *Figures 4 and 5. Please provide details in the main text:*

- *Are the data interpolated before EMD analysis? If yes, how?*

- *How are computed the spectrum and the confidence level at the right of each IMF?*

- *Are the results different if the frequency range for each IMF is changed? Please, show it.*

Reply: a. We linearly interpolated the raw loess and speleothem data by 0.1-kyr interval before EMD analysis.

b. We performed Redfit for every IMF component, the confidence level can be directly acquired using Redfit software.

We clarified these two issues in lines 24-26, page 5 and lines 24-25, page 6.

c. We do not quite understand this question. The frequency range is based on the spectral result of corresponding IMF, and thus can not be changed subjectively. Indeed, we did not set any frequency band before the decomposition procedure.

8. *Figure 6.*

- *Apply to the LR04 time series the same filtering procedure as for MGS and Speleothem data, in order to compare signals filtered in the same way.*

- *In section 4.1 of the manuscript, the authors write that $d18O$ from speleothem « varies quite synchronously with the July insolation ». I agree with that. It's quite clear from a visual inspection on figure 6. They also claim for a good correlation between the LR04 time series and the MGS record. There, a more quantitative analysis than visual inspection is required.*

Reply: a. The objective of this study is to evaluate the orbital discrepancy and millennial similarity between loess grain size and speleothem $\delta^{18}O$ records and to address the driving force for East Asian monsoon variations on different timescales. One efficient way is to directly compare the orbital and millennial components of loess grain size and speleothem $\delta^{18}O$ series with potential forcing (e.g., solar insolation and ice volume) changes. In addition, since the millennial signals in LR04 is rather limited, we still keep the LR04 as a proxy indicator of the ice volume forcing in Figure 6.

b. We did linear regression between orbital signal of MGS and LR04 records, the R^2 is 0.536.

The value is not high because global ice volume is not the unique driver of low-frequency signal of East Asian monsoon. We wrote that “Gulang MGS record is well correlated with global ice volume change inferred from the benthic $\delta^{18}\text{O}$ record” because both of these two records share similar glacial-interglacial contrast (see lines 20-24, page 7).

9. *Figure 7.*

- *Are the three signals identically filtered?*

- *You write « YD and Heinrich events recorded in the three records ». How? Do they occur EXACTLY at the same age in the time series, as it is implicitly suggested on the figure?*

- *You write « gray bars indicate interglacial periods » ; interglacial???*

- *How do you settle the « interstadial numbers »?*

Reply: a. We did not filter the raw data by given frequency bands. We performed EMD to directly get intrinsic model function (IMF) components, and combined components with periodicity no more than 10 kyr together as millennial-scale signals.

b. The YD and Heinrich-like events at around 12, 16, 24, 31, 39, 48, 55, and 60 kyr in Figure 7 have generally obvious counterpoints of coarse grain sizes in Gulang and CHILOMOS stack records and heavy $\delta^{18}\text{O}$ values in Sanbao/ Hulu speleothem series, though the timing of coarsening grain size around 48 kyr in the CHILOMOS stack record is slightly mismatched relative to the H₅ event.

c. The gray bars in Figure 7 have already been corrected.

d. The interstadial numbers of speleothem $\delta^{18}\text{O}$ and CHILMOMOS stack records have been published in papers of [Wang et al., 2008](#) and [Yang and Ding, 2014](#), respectively. We marked the numbers for speleothem and CHILMOMOS records at roughly similar ages according to the above two references, and marked the numbers on fine particle size peaks at corresponding ages for Gulang grain size record.

10. *A more quantitative analysis is required for the last section (section 4.2 about the millennial oscillations).*

- *page 11, row 11/12: « ... are well aligned with comparable amplitude and duration ».*

Please perform a quantitative analysis to compare them.

- As indicated above, the detection of the Heinrich and YD events in the records is not clear to me.

Reply: a. Thank you for this suggestion. The description of “comparable amplitude” between Gulang loess and speleothem records, which has been deleted in the revised manuscript, is not sufficiently rigorous. However, the similar duration can be obviously detected by visual inspection.

b. Again, after the reinterpretation of Gulang particle size data, the YD and Heinrich events correlated well with coarse particle size and heavy speleothem $\delta^{18}\text{O}$ signals (See Figure 7).

11. Typing comments:

- Page 3, row 19: and -> but (?)

- Page 6, row 10: space -> sampled

- Page 8, row 20: >10kyr -> period>10kyr

- Legend of figure 2: Isiecki -> Lisiecki

Reply: All the above typing errors have been corrected in the revised manuscript.

Cpd-2014-135-referee-report-4

1. In order to verify and support the results, I suggested to use a method not related to the Fourier approach, but the Authors applied MTM (although implemented in the same toolkit together with SSA and MEM, it is substantially based on the Fourier transform). Moreover, the Monte Carlo test I suggested (more specific in respect to that used by the Authors also in the revised version) was not applied.

Reply: Thanks to the reviewer’s comment, I spent a relatively long time to learn about SSA toolkit since it had been an entirely unfamiliar program to me. As far as I concern, among programs implemented in SSA-MTM toolkit, MTM is the method for spectral analysis of a

time series, and this is the reason why we used MTM to compare with REDFIT spectral results.

As the referee suggested, we applied SSA method to decompose our Gulang MGS data, however, more than 10 components at millennial bands were decomposed from the original data. Moreover, due to the limited period of revising process, the concept of Monte Carlo test is still inexplicit to us. Because EMD method has been employed intensively for decomposing multiple components of paleoclimatic records (Gloersen and Huang, 2003; Hu and Wu, 2004; Lin and Wang, 2006; Molla et al., 2006; Cai et al., 2015), we still employed the EMD method in our revised manuscript.

2. Regarding the components extracted from the series, the authors used EMD to avoid the arbitrariness in the choice of frequency bands. However, IMF1 to 6 in Fig. 4(A) and 5(A) clearly show that each component contains a broad range of oscillations of different frequency. E.g., in IMF3 of Fig.4 the ‘dominant’ period of 16 ky present in the spectrum on the right is due to the single event at about 100 ky BP. Therefore it is not correct to associate the variance of 6% to an oscillation component of 16 ky. Also IMF5 in Fig. 4(A) contains only one ‘event’ lasting about 40 ky and many oscillations of period of about 23 ky. So the variance associated to 23 ky is actually contained partly in IMF4 and partly in IMF5. Therefore different variability modes are not well separated in different components.

Reply: EMD is a widely used decomposing approach among palaeoclimate database, such as ice-cover (Gloersen and Huang, 2003), North Atlantic oscillation (Hu and Wu, 2004), solar insolation (Lin and Wang, 2006), Indian monsoon (Cai et al., 2015), and temperature under global warming (Molla et al., 2006). For the purpose of comparing with other paleoclimatic records, we prefer to use the EMD to decompose multi-scale variability.

In the revised manuscript, Gulang grain size data was reanalyzed based on the updated chronology of Sun et al., 2015. Meanwhile, the EMD code was slightly amended to better separate components. Thus, IMFs of loess and speleothem records and corresponding dominant periodicities of each IMF were changed accordingly in Figure 4 and 5. The revised orbital component (IMF4) of Gulang particle size record show both 23 and 41 kyr

periodicities, and other IMF oscillations are generally at the corresponding period pace (see Figure 4). Here we clarified that the revised components at various timescales are well separated from the raw loess and speleothem records.

3. 80% of *c. l.* is a low value. It would be interesting to specify which components remain significant at a higher *c. l.*, e.g. 90 or 95%. In Fig. 3 they show the 80% *c. l.* for the REDFIT spectrum (as in the previous version) and 90% *c. l.*, but for MTM.

Reply: From Figure R1, we found that for the Gulang particle size record, the periodicities of 100kyr, 23kyr, and 5-1kyr are significant at 90% level while only 100kyr and 2-1kyr are detected at 95% significance level; for the speleothem $\delta^{18}\text{O}$ record, the 23kyr period is absolutely dominant since the peak exceeds a lot even from 95% significance level.

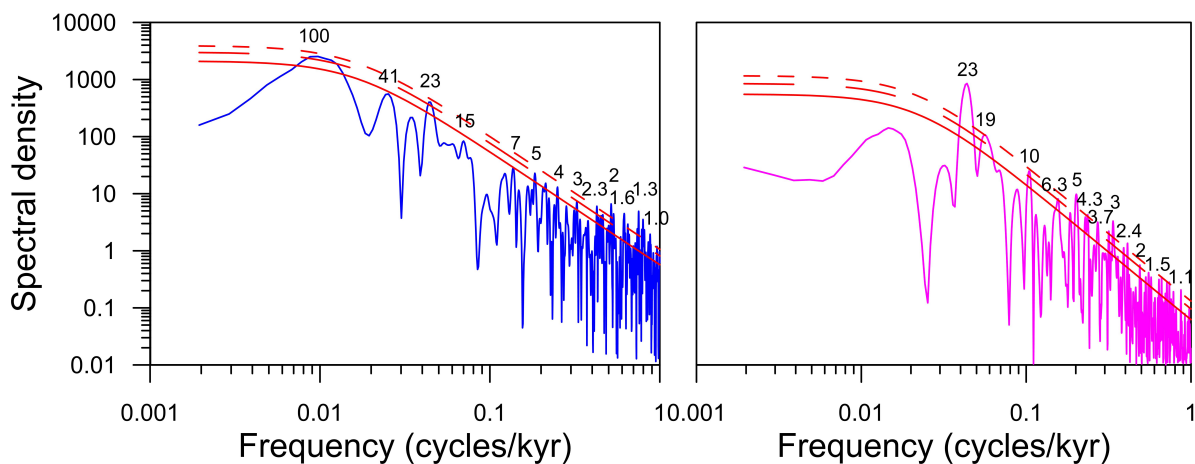


Figure R1. Spectrum results of Gulang MGS (left) and Sanbao/Hulu speleothem $\delta^{18}\text{O}$ (right) (Wang et al., 2008; Cheng et al., 2009) records using REDFIT method. The red solid, long dashed, and short dashed lines represent 80%, 90%, and 95% confidence levels. Periodicities are shown above the spectral curves.

References

- Cheng, H., Edwards, R. L., Broecker, W. S., Denton, G. H., Kong, X., Wang, Y., Zhang, R., and Wang, X.: Ice age terminations, *Science*, 326, 248–252, 2009.
- Liang, L., Sun, Y., Yao, Z., Liu, Y., and Wu, F.: Evaluation of high-resolution elemental analyses of Chinese loess deposits measured by X-ray fluorescence core scanner, *Catena*, 92, 75-78, 2012.
- Sun, Y., Clemens, S. C., Morrill, C., Lin, X., Wang, X., and An, Z.: Influence of Atlantic meridional overturning circulation on the East Asian winter monsoon, *Nat Geosci*, 5, 46–49, 2012.
- Sun, Y., Kutzbach, J., An, Z., Clemens, S., Liu, Z., Liu, W., Liu, X., Shi, Z., Zheng, W., Liang, L., Yan, Y., and Li, Y.: Astronomical and glacial forcing of East Asian summer monsoon variability, *Quaternary Sci. Rev.*, 115, 132-142, 2015.
- Wang, Y., Cheng, H., Edwards, R. L., Kong, X., Shao, X., Chen, S., Wu, J., Jiang, X., Wang, X., and An, Z.: Millennial and orbital-scale changes in the East Asian monsoon over the past 224,000 years, *Nature*, 451, 1090–1093, 2008.
- Yang, S. and Ding, Z.: A 249 kyr stack of eight loess grain size records from northern China documenting millennial-scale climate variability, *Geochem. Geophys. Geosy.*, 15, 798–814, 2014.
- Gloersen, P. and Huang, N.: Comparison of interannual intrinsic modes in hemispheric ice covers and other geophysical parameters, *IEEE Transactions in Geosciences and Remote Sensing*, 41, 1062-1074, 2003.
- Hu, Z. and Wu, Z.: The intensification and shift of the annual North Atlantic Oscillation in a global warming scenario simulation, *Tellus*, 56, 112-124, 2004.
- Lin, Z. and Wang, S.: EMD analysis of solar insolation, *Meteorol. Atmos. Phys.*, 93, 123-128, 2006.
- Molla, K., Sumi, A., and Rahman, M.: Analysis of temperature change under global warming impact using Empirical Mode Decomposition, *Int. J. Information Technol.*, 3, 131-139, 2006.
- Cai, Y., Fung, I. Y., Edwards, R. L., An, Z., Cheng, H., Lee, J. E., Tan, L., Shen, C. C., Wang, X., Day, J. A., Zhou, W. J., Kelly, M. J., and Chiang, J. C. H.: Variability of

stalagmite-inferred Indian monsoon precipitation over the past 252,000 y, Proc. Natl. Acad. Sci. U. S. A., 112, 2954-2959, 2015.

A list of relevant changes

We have revised this manuscript greatly according to the reviewers' insightful comments, including a description of the grain size chronology construction (line 29, page 3, and lines 1-4, page 4), spectral and decomposing results (lines 24-29, page 6, and lines 1-10, page 7). All relevant changes are highlighted in the manuscript below.

1 **Abstract**

2 The East Asian Monsoon exhibits a significant variability on timescales ranging from tectonic
3 to centennial as inferred from loess, speleothem and marine records. However, the relative
4 contributions and plausible driving forces of the monsoon variability at different timescales
5 remain controversial. Here, we spectrally explore time series of loess grain size and
6 speleothem $\delta^{18}\text{O}$ records and decompose the two proxies into intrinsic components using
7 Empirical Mode Decomposition method. Spectral results of these two proxies display clear
8 glacial-and-orbital periodicities corresponding to ice-volume and orbital cycles, and evident
9 millennial signals which are in pace with Heinrich rhythm and DO cycles. Six intrinsic
10 components are parsed out from loess grain size and speleothem $\delta^{18}\text{O}$ records, respectively,
11 and combined signals are correlated further with possible driving factors including the ice
12 volume, insolation and North Atlantic cooling. The relative contributions of six components
13 differ significantly between loess grain size and speleothem $\delta^{18}\text{O}$ records. Coexistence of
14 glacial and orbital components in the loess grain size implies that both ice volume and
15 insolation have distinctive impacts on the winter monsoon variability, in contrast to the
16 predominant precessional impact on the speleothem $\delta^{18}\text{O}$ variability. Moreover, the millennial
17 components are evident with variances of 13 % and 17 % in loess grain size and speleothem
18 $\delta^{18}\text{O}$ records, respectively. A comparison of the millennial-scale signals of these two proxies
19 reveals that abrupt changes in the winter and summer monsoons over the last 260 kyr share
20 common features and similar driving forces linked to high-latitude Northern Hemisphere
21 climate.

22

23 **1 Introduction**

24 The East Asian Monsoon (EAM), as a significant part of Asian monsoon circulation, plays an
25 important role in driving the palaeoenvironmental changes in East Asia (An, 2000). The
26 EAM fluctuations can be quantified at different time intervals ranging from thousands of
27 years to intraseasonal periodicities, and the primary driving force of the monsoon variability
28 on each timescale is not unique (An et al., 2015). Multiscale monsoon variability has been
29 inferred from numerous proxies generated from deep-sea sediments (e.g., Wang et al., 1999;

1 Wang et al., 2005), eolian deposits (e.g., An, 2000, Sun et al., 2012), and speleothem records
2 (e.g., Wang et al., 2001, 2008), which provide valuable insights into the changing processes
3 and potential driving forces of the EAM variability. In particular, Chinese loess has been
4 investigated intensively as a direct and complete preserver of the EAM changes, with great
5 efforts on deciphering on the EAM variability on both orbital and millennial scales (e.g., An
6 et al., 1990; Ding et al., 1994, 2002; Porter and An, 1995; Guo et al., 1996; Chen et al., 1997;
7 Liu and Ding, 1998; Liu et al., 1999; An, 2000; Chen et al., 2006).

8 On the orbital timescale, the EAM variation recorded by Chinese loess-paleosol sequences
9 was characterized by an alternation between the dry-cold winter monsoon and the wet-warm
10 summer monsoon (Liu and Ding, 1998; An, 2000). A strong 100 kyr periodicity was detected
11 in the Chinese loess particle size record, implying an important impact of glacial boundary
12 conditions on the EAM evolution (Ding et al., 1995). Obliquity and precession signals were
13 also clear in loess based proxies (Liu et al., 1999; Ding et al., 2002; Sun et al., 2006). Apart
14 from these dominant periodicities, some harmonic periodicities related to orbital parameters
15 were also found in the EAM records, such as the ~75, ~55, and ~30 kyr spectral peaks (Lu et
16 al., 2003; Sun et al., 2006; Yang et al., 2011). In contrast, absolute-dated speleothem $\delta^{18}\text{O}$
17 records revealed an evident 23 kyr cycle, implying a dominant role of summer insolation in
18 driving the summer monsoon variability (Wang et al., 2008; Cheng et al., 2009). Different
19 variances of obliquity and precession signals in monsoonal proxies suggest that the responses
20 of the winter and summer monsoons to the orbital forcing were dissimilar (Shi et al., 2011).
21 The various patterns of orbital-scale monsoon fluctuations between the loess proxies and
22 speleothem $\delta^{18}\text{O}$ records likely reflected the sensitivity of various archives and proxies to the
23 EAM variability (Clemens et al., 2010; Cheng et al., 2012; Sun et al., 2015; Cai et al., 2015).

24 At the millennial timescale, the rapid monsoon oscillations inferred from Chinese loess were
25 not only persistent during the last two glacial cycles (Porter and An, 1995; Guo et al., 1996;
26 An and Porter, 1997; Chen et al., 1997; Ding et al., 1999; Sun et al., 2010; Yang and Ding,
27 2014), but were also evident during early glacial extreme climatic conditions (Lu et al., 1999).
28 The millennial-scale monsoon variability during the last glacial period was strongly coupled
29 to climate changes recorded in Greenland ice-core and North Atlantic sediments, indicating a

1 dynamic connection between the EAM variability and the high-latitude Northern Hemisphere
2 climate (Porter and An, 1995; Guo et al., 1996; Chen et al., 1997; Fang et al., 1999). Recently,
3 a combination of proxies from Chinese loess, speleothem, and Greenland ice-core with
4 modeling results indicated that the Atlantic meridional overturning circulation might have
5 played an important role in driving the rapid monsoon changes in East Asia during the last
6 glaciation (Sun et al., 2012).

7
8 Though previous studies have revealed that past EAM variabilities principally comprise a
9 mixture of forcing signals from ice volume, solar radiation, and North Atlantic climate, the
10 relative contributions of glacial, orbital and millennial forcing to the EAM variability remain
11 unclear. In this study, we conducted a comprehensive investigation of multiscale EAM
12 variability over the last 260 kyr, by analyzing mean grain size (MGS) record from a Gulang
13 loess sequence (a proxy indicator of the East Asian winter monsoon intensity) and
14 speleothem $\delta^{18}\text{O}$ record of Hulu and Sanbao caves (a debatable indicator of the summer
15 monsoon intensity). Our objectives are to evaluate the relative contributions of
16 glacial–interglacial to millennial signals registered in these two widely employed monsoon
17 proxies, and to emphasize the glacial-interglacial discrepancy and millennial similarity
18 between loess and speleothem records during the last two glacial cycles.

19 20 **2 Data and methods**

21 The data for the loess sequence was collected at a section in Gulang, Gansu Province, China
22 (37.49°N, 102.88°E, 2400 ma.s.l.), which is situated in the northwestern part of the Chinese
23 Loess Plateau. It is about 10 km to the southwest margin of the Tengger desert (Fig. 1). In
24 this region, the average annual precipitation and temperature over the last 20 years are 350
25 mm and 5.7 °C, respectively. About 70 m loess was accumulated at Gulang during the last
26 two climate cycles. High sedimentation rate and weak pedogenesis in this region make the
27 Gulang loess sequence very sensitive to orbital and millennial monsoon changes (Sun et al.,
28 2012, 2015). The samples used in this study were collected at 2cm intervals, corresponding to
29 50–100 yr resolution for the loess-paleosol sequence. The grain size data of the upper 20 m

1 were from a 20-m pit near Gulang (Sun et al., 2012), and the lower part spanning the last two
2 glacial cycles was from another 50-m section. Mean grain size data of the composite 70-m
3 section have been employed for a chronological reconstruction (for a detailed description, see
4 Sun et al., 2015). The Gulang chronology was evaluated by comparison with a 249-kyr grain
5 size stack (CHILOMOS) record in the northern Loess Plateau (Yang and Ding, 2014) (Fig.2);
6 the good matches between these two records imply a high reliability of our Gulang age
7 construction. Unlike previous studies (Sun et al., 2012, 2015), we performed spectral and
8 decomposing analysis on the mean grain size time series in order to decipher multiscale
9 variability and dynamics of the winter monsoon.

10 The absolute-dated speleothem $\delta^{18}\text{O}$ records from Sanbao/Hulu caves (0-224 kyr, Wang et al.,
11 2008) and the Sanbao cave (224-260 kyr, Cheng et al., 2009) (Fig. 1) were selected to infer
12 summer monsoon variability spanning the last two glacial–interglacial cycles. Compatible
13 with the analysis by Wang et al (2008), we plot the Hulu $\delta^{18}\text{O}$ data 1.6‰ more negative than
14 that from the Sanbao cave (Fig. 2). Interpretation of the Chinese speleothem $\delta^{18}\text{O}$ records
15 remains debatable as a direct indicator of summer monsoon intensity since various factors
16 like seasonal changes in precipitation amount, moisture sources, and circulation patterns
17 would influence the speleothem $\delta^{18}\text{O}$ composition (e.g., Yuan et al., 2004; Wang et al., 2001,
18 2008; Cheng et al., 2009; Clemens et al., 2010; Dayem et al., 2010; Pausata et al., 2011;
19 Maher and Thompson, 2012; Caley et al., 2014). Nevertheless, high similarity between
20 millennial events in Chinese speleothem and Greenland ice core revealed that speleothem
21 $\delta^{18}\text{O}$ is a reliable indicator of seasonal monsoon change (Wang et al., 2001; Clemens et al.,
22 2010). More recently, a model-data comparison suggested that Chinese speleothem $\delta^{18}\text{O}$ can
23 be regarded as a monsoon proxy to reflect the southerly wind intensity rather than the
24 precipitation change (Liu et al, 2014). Thus, spectral and decomposed results of the
25 composite speleothem $\delta^{18}\text{O}$ record time series were used in this study to address multiscale
26 variability and dynamics of the summer monsoon.

27 To detect the presence of glacial-to-millennial periodicities, we performed spectral analysis
28 on the 260 kyr records of Gulang MGS and speleothem $\delta^{18}\text{O}$ using both of Multitaper (MTM,
29 implemented in the SSA toolkit, Vautard et al., 1992) (<http://www.atmos.ucla.edu/tcd/ssa/>)

1 and REDFIT (Schulz and Mudelsee, 2002) methods, which are related to Empirical
2 Orthogonal Function and Lomb–Scargle Fourier transform, respectively. MTM method has
3 the advantages of quantified and optimized trade-off between spectral leakage reduction and
4 variance reduction and being suitable for series affected by high-noise levels (Lu et al., 1999),
5 but MTM requires equally-spaced data and therefore an interpolation is needed. The REDFIT
6 program estimates the first-order autoregressive (AR1) parameter from unevenly sampled
7 time series without interpolation, which avoids a too “red” spectrum (Schulz and Stattegger,
8 1997), but uses WOSA methods for spectral leakage reduction and variance reduction, which
9 makes the trade-off not quantifiable. The similar spectral periodicities derived from both
10 REDFIT and MTM methods were regarded as dominant frequencies at glacial-to-millennial
11 bands.

12 The decomposed components of loess MGS and speleothem $\delta^{18}\text{O}$ records were parsed out
13 using the technique of Empirical Mode Decomposition (EMD) (Huang et al., 1998). EMD
14 directly extracts energy which is associated with intrinsic time scales in nonlinear fluctuations,
15 and iteratively decomposes the raw complex signal with several characteristic time scales
16 coexisting into a series of elementary intrinsic model function (IMF) components, avoiding
17 any arbitrariness in the choices of frequency bands in this multiscale study. The EMD method
18 has been widely employed over various palaeoclimate database, such as ice-cover (Gloersen
19 and Huang, 2003), North Atlantic oscillation (Hu and Wu, 2004), solar insolation (Lin and
20 Wang, 2006), and temperature under global warming (Molla et al., 2006). This approach has
21 also been used to decipher the multiscale variations of Indian monsoon (Cai et al., 2015).
22 However, the application of EMD method on the loess record remains poorly investigated
23 with limited understanding of decomposed components at glacial-and-orbital timescales due
24 to the low-resolution proxy variations (Yang et al., 2001, 2008). In this study, we applied
25 EMD on interpolated loess and speleothem data with 100 yr interval to quantify the relative
26 contributions of both orbital and millennial components.

27 28 **3 Multiscale monsoon variability**

29 The highly comparable spectral results between REDFIT and MTM methods show that

1 apparent periods identified in the MGS spectrum are at ~100, ~41, ~23, ~15, ~7, ~5, ~4, and
2 ~3-1 kyr over the 80 % and 90 % confidence levels, respectively, for REDFIT and MTM
3 methods (Fig. 3). It is shown that the potential forcing of the glacial–interglacial and orbital
4 EAM variability is part of the external (e.g., the orbital-induced summer insolation, [An, 1991](#);
5 [Wang et al., 2008](#)) and the internal factors (e.g., the changes in the ice volume and CO₂
6 concentrations, [Ding et al., 1995](#); [Lu et al., 2013](#); [Sun et al., 2015](#)). The coexistence of the
7 ~100, ~41, and ~23 kyr periods in the Gulang MGS record confirms the dynamic linkage of
8 the winter monsoon variability to glacial and orbital forcing. Based on the spectral results,
9 many millennial frequencies are detected, which can be mainly divided into two groups of
10 ~7-4 and ~3-1 kyr, which, possibly correspond, respectively, to the Heinrich (~6 kyr) rhythm
11 and the Dansgaard–Oeschger (DO, ~1.5 kyr) cycles recorded in the North Atlantic sediments
12 and Greenland ice core ([Bond et al., 1993](#); [Dansgaard et al., 1993](#); [Heinrich, 1988](#)). Taking
13 into account the sampling resolution and surface mixing effect at Gulang, the residual
14 component (< 1 kyr) might contain both centennial and noisy signals, which is excluded for
15 further discussion in this study.

16 Compared to the MGS spectral results, the speleothem $\delta^{18}\text{O}$ spectrum shares similar peaks at
17 the precession (~23 kyr) and millennial bands (~5, ~3, ~2.4, ~2, ~1.5, ~1.3, and ~1 kyr), but
18 is lack of distinct peaks at ~100 kyr and ~41 kyr (Fig. 3). Notably, precession peaks at ~23
19 and ~19 kyr are more dominant in the speleothem $\delta^{18}\text{O}$ than in the loess MGS record.
20 Moreover, the speleothem spectrum shows a peak over the 80 % and 90 % confidence levels
21 in REDFIT and MTM spectrum, respectively, centered at ~10 kyr frequency, which is,
22 approximately, related to the semi-precession frequency.

23 The different oscillation patterns composing loess MGS and speleothem $\delta^{18}\text{O}$ time series are
24 separated out using EMD method as presented in Fig. 4 and Fig. 5, respectively. Redfit
25 spectral analysis are further conducted on each IMF with with dominant periods as shown.
26 Five IMFs are generated for the Gulang MGS data on glacial-to-millennial timescale. The
27 variability of Gulang MGS is dominated by the lowest frequency signal with variances of 32
28 % (IMF5). Two periodicities (41 kyr and 23 kyr) in orbital component (IMF4) are linked to
29 obliquity and precession, contributing altogether 40 % to the total variance. The periodicities

1 in IMF3 dominated by 15-kyr periodicity likely correspond to the second precessional cycle.
2 The variances of two millennial components (IMF2 and IMF1) are very close with variances
3 of 8 % and 5 %, respectively, in the Gulang MGS record. Similarly, six IMFs are
4 decomposed for the speleothem $\delta^{18}\text{O}$ record on frequencies lower than 1 kyr, and all the
5 glacial-to-orbital periodicities correspond to Milankovitch parameters. Compared with
6 decomposed results of Gulang MGS record, glacial (IMF6) and obliquity (IMF5) components
7 are not clear in the speleothem $\delta^{18}\text{O}$ record with variances of 12 %, respectively. The
8 precession component (IMF4), however, is the most dominant signal among the six
9 components, accounting for 59 % of the variance. Notable millennial components (IMF3, 2,
10 and 1) are evident with variances of 8 %, 6 % and 3 %, respectively.

11 **4 Dynamics of multiscale EAM variability**

12 **4.1 Glacial and orbital forcing of the EAM variability**

13 We combine IMF3, 4, and 5 of Gulang MGS and IMF 4, 5, and 6 of speleothem $\delta^{18}\text{O}$ records
14 as the low-frequency signals (period > 10 kyr) to reveal the glacial-and-orbital scale variations
15 of the winter and summer monsoon, respectively. The glacial-and-orbital variations of the
16 loess and speleothem records represent the total variances of ~87 % and ~83 %, respectively.
17 The low-frequency signals of the loess MGS and speleothem $\delta^{18}\text{O}$ records are compared with
18 changes in the ice volume and solar insolation at 65°N (Berger, 1978) to ascertain plausible
19 impacts of glacial and orbital factors on the EAM variability (Fig. 6).

20 The low-frequency component of the Gulang MGS record is well correlated to global ice
21 volume change inferred from the benthic $\delta^{18}\text{O}$ record (Lisiecki and Raymo, 2005) with
22 correlation coefficient (R^2) of 0.56, reinforcing the strong coupling between the winter
23 monsoon variation and ice-volume changes, particularly in terms of glacial-interglacial
24 contrast, (Ding et al., 1995). However, fine MGS signals at the precessional scale seem more
25 distinctive than those in the benthic $\delta^{18}\text{O}$ stack. For example, the remarkable peaks in the
26 MGS around 50, 85, 110, and 170 kyr have no counterpoints in the benthic $\delta^{18}\text{O}$ record. By
27 comparing MGS data with the summer insolation record, the overall ~20 kyr periodicity is
28 damped but still visible during both glacial and interglacial periods, except for insolation

1 maxima around 150 and 220 kyr (Fig. 6). The coexistence of the glacial and orbital cycles in
2 loess MGS indicates that both the ice volume and solar insolation have affected the winter
3 monsoon variability, and their relative contributions are 32 % and 55 %, respectively, as
4 estimated from variances of the glacial (IMF5) and orbital (IMF4 and 3) components.

5 The speleothem $\delta^{18}\text{O}$ record varies quite synchronously with the July insolation,
6 characterized by a dominant precession frequency (Fig. 6). This in-phase change is thought to
7 support a dominant role of summer insolation in the Northern Hemisphere in driving the
8 summer monsoon variability at the precession period (Wang et al., 2008), given that the
9 palaeoclimatic interpretation of the speleothem $\delta^{18}\text{O}$ is quite controversial (Wang et al., 2001,
10 2008; Yuan et al., 2004; Hu et al., 2008; Cheng et al., 2009; Peterse et al., 2011).

11 The different contributions of glacial and orbital variability in the loess MGS and speleothem
12 $\delta^{18}\text{O}$ records indicate that the driving forces associated with these two proxies are different.
13 The loess grain size is directly related to the northwesterly wind intensity, reflecting that
14 atmospheric surface process is linked to the Siberian-Mongolian High (Porter and An, 1995).
15 The speleothem $\delta^{18}\text{O}$ might be influenced by multiple factors such as the isotopic depletion
16 along the vapor transport path (Pausata et al., 2011), changes in $\delta^{18}\text{O}$ values of meteoric
17 precipitation or the amount of summer monsoon precipitation (Wang et al., 2001, 2008;
18 Cheng et al., 2009), and seasonality in the amount and isotopic composition of rainfall
19 (Clemens et al., 2010; Dayem et al., 2010; Maher and Thompson, 2012). Even at the orbital
20 timescale, proxy-model comparison suggested that the response of the winter and summer
21 monsoon to obliquity and precession forcing are dissimilar (Shi et al., 2011)

22 It is quite clear that the EAM is formed by the thermal gradient between the Asian continent
23 and the Pacific Ocean to the east and southeast (Halley, 1986; Xiao et al., 1995; Lestari and
24 Iwasaki, 2006). In winter, due to a much larger heat capacity of water in the ocean than that
25 on the land surface, a higher barometric pressure forms over the colder Asian continent with a
26 lower pressure over the warmer ocean. This gradient is the driving force for the flow of cold
27 and dry air out of Asia, consequently, the winter monsoon forms (Gao, 1962). On the
28 glacial–interglacial timescale, the buildup of the northern high-latitude ice sheets during the
29 glacial periods strengthens the barometric gradient which results in intense winter monsoons

1 (Ding et al., 1995; Clark et al., 1999). The contemporaneous falling sea level and land-ocean
2 pressure gradient further enhances winter monsoon circulation during glacial times (Xiao et
3 al., 1995). The other factor that influences the land-ocean differential thermal motion is the
4 orbitally induced solar radiation changes. The precession-induced insolation changes can lead
5 to regional land-ocean thermal gradients whilst obliquity-related insolation changes can result
6 in meridional thermal gradients; both of which can substantially alter the evolution of the
7 Siberian and Subtropical Highs and the EAM variations (Shi et al., 2011).

8 **4.2 Impacts of high-latitude cooling on millennial EAM oscillations**

9 The EAM variations are persistently punctuated by apparent millennial-scale monsoon events
10 (Garidel-Thoron et al., 2001; Wang et al., 2001; Kelly et al., 2006). The millennial-scale
11 events of the last glacial cycle were firstly identified in Greenland ice cores (Dansgaard et al.,
12 1993; Meese et al., 1997). Subsequently, well-dated loess grain size and speleothem $\delta^{18}\text{O}$
13 records in China have been found to have apparent correspondences with rapid climate
14 oscillations in the North Atlantic (Porter and An, 1995; Guo et al., 1996; Chen et al., 1997;
15 Ding et al., 1998; Wang et al., 2001). The most striking evidence is the strong correlation
16 between the loess grain size, speleothem $\delta^{18}\text{O}$ and Greenland ice core $\delta^{18}\text{O}$ records during the
17 last glaciation (Ding et al., 1998; Wang et al., 2001; Sun et al., 2012). These abrupt changes
18 have been extended into the past glacial–interglacial cycles from loess and speleothem
19 records (Ding et al., 1999; Cheng et al., 2006, 2009; Wang et al., 2008; Yang and Ding, 2014)
20 and from the North Atlantic sediments (McManus et al., 1999; Channell et al., 2012).

21 Unlike previous comparison based on original proxy variability, here we combine the IMF1
22 and 2 components of the loess MGS and IMF1, 2, and 3 components of speleothem $\delta^{18}\text{O}$
23 records as robust reflection of millennial-scale signals of the winter and summer monsoons,
24 with variances of 13 % and 17 %, respectively. The combination of the two millennial signals
25 of the loess MGS and speleothem $\delta^{18}\text{O}$ records are compared further with the North Atlantic
26 cooling events over the last two glacial cycles, to reveal the dynamic links of abrupt climate
27 changes in East Asia and the North Atlantic (Fig. 7). The Younger Dryas (YD) and Heinrich
28 Events (H_1 - H_6) are well detected in loess and speleothem records around 12, 16, 24, 31, 39,

1 48, 55, and 60 kyr, respectively. Most of the millennial-scale events in the loess MGS and
2 speleothem $\delta^{18}\text{O}$ records are well aligned with comparable timing and duration during the last
3 two glacial cycles. However, some MGS valleys such as A17, A23, B17, B18, and B22 are
4 not well matched with the speleothem $\delta^{18}\text{O}$ minima, possibly due to uncertainties in the loess
5 chronology. The comparable millennial scale events between grain size of Gulang and
6 CHILOMOS stack (Yang and Ding, 2014) shows the nature of replication of Gulang MGS
7 record within the dating uncertainty, confirming the persistent millennial-scale winter
8 monsoon variability spanning the last two glacial cycles (Fig. 7).

9 The millennial-scale monsoon signals over the last two glacial cycles have been well
10 compared with the cooling events recorded in the North Atlantic sediments, demonstrating a
11 dynamic link between abrupt climate changes in East Asia and the North Atlantic. As
12 identified in Chinese speleothem records, the magnitudes of abrupt climate events are
13 identical between the last and the penultimate climatic cycles (Wang et al., 2008). However,
14 the duration and amplitude of these millennial events seems quite different between the
15 glacial and interglacials. The duration of millennial monsoon events is relatively shorter and
16 the amplitude larger during glacial periods, suggesting a plausible glacial modulation on
17 rapid climate changes (McManus et al., 1999; Wang et al., 2008). The potential driving
18 mechanism for rapid EAM changes has been attributed to changing climate in the
19 high-latitude Northern Hemisphere, e.g., the reduction of the North Atlantic deep water
20 circulation triggered by fresh water inputs from melting icebergs (Broecker, 1994). The North
21 Atlantic cooling can affect the zonal high pressure systems, including the Azores-
22 Ural-Siberian-Mongolian high (Palmer and Sun, 1985; Rodwell et al., 1999; Yuan et al.,
23 2004), which can further transmit the abrupt cooling effect into East Asia and result in
24 significant EAM changes (Porter and An, 1995; Wang et al., 2001). Apart from the
25 geological evidence, numerical modeling also suggests that the Atlantic meridional
26 overturning circulation might affect abrupt oscillations of the EAM, while the westerly jet is
27 the important conveyor introducing the North Atlantic signal into the EAM region (Miao et
28 al., 2004; Zhang and Delworth, 2005; Jin et al., 2007; Sun et al., 2012).

29

1 **5 Conclusions**

2 The multiscale signals were spectrally detected and naturally decomposed from Chinese loess
3 and speleothem records over the last two climatic cycles, permitting an evaluation of the
4 relative contributions of glacial, orbital and millennial components in the EAM record.
5 Spectrum of Gulang MGS and speleothem $\delta^{18}\text{O}$ data show similar periodicities at
6 glacial-to-orbital and millennial timescales, corresponding to the rhythms of changing
7 ice-volume, orbitally induced insolation, and North Atlantic cooling (i.e., Heinrich rhythm
8 and Dansgaard–Oeschger cycles), respectively. Amplitude variances of the decomposed
9 components reveal significant glacial and orbital impacts on the loess grain size variation and
10 a dominant precession forcing in the speleothem $\delta^{18}\text{O}$ variability. The millennial components
11 are evident in the loess and speleothem proxies with variances of 13 % and 17 %,
12 respectively. Millennial IMFs were combined to recognize the synchronous nature of rapid
13 changes of these two proxies. High similarity of millennial-scale monsoon events both in
14 terms of the rhythms and duration between the loess and speleothem proxies implies that the
15 winter and summer monsoons share common millennial features and similar driving forces.

16

17 **Acknowledgements**

18 Four anonymous reviewers and Dr. Loutre Marie-France are acknowledged for their
19 insightful comments. This work was supported by funds from the National Basic Research
20 Program of China (2013CB955904), the Chinese Academy of Sciences (KZZD-EW25
21 TZ-03), the National Science Foundation of China (41472163), and the State Key Laboratory
22 of Loess and Quaternary Geology (SKLLQG1011).

1 **References**

2 An, Z. and Porter, S. C.: Millennial-scale climatic oscillations during the last interglaciation
3 in central China, *Geology*, 25, 603–606, 1997.

4 An, Z., Liu, T., Lu, Y., Porter, S. C., Kukla, G., Wu, X., and Hua, Y.: The long-term
5 paleomonsoon variation recorded by the loess-paleosol sequence in Central China, *Quatern.
6 Int.*, 7, 91–95, 1990.

7 An, Z., Wu, G., Li, J., Sun, Y., Liu, Y., Zhou, W., Cai, Y., Duan, A., Li, L., Mao, J., Cheng,
8 H., Shi, Z., Tan, L., Yan, H., Ao, H., Chang, H., and Juan, F.: Global monsoon dynamics and
9 climate change, *Annu. Rev. Earth. Planet. Sci.*, 42,
10 doi:10.1146/annurev-earth-060313-054623, 2015.

11 An, Z.: Magnetic susceptibility evidence of monsoon variation on the Loess Plateau of
12 central China during the last 130,000 years, *Quaternary Res.*, 36, 29–36, 1991.

13 An, Z.: The history and variability of the East Asian paleomonsoon climate, *Quaternary Sci.
14 Rev.*, 19, 171–187, 2000.

15 Berger, A.: Long-term variations of daily insolation and Quaternary climate changes, *J.
16 Atmos. Sci.*, 35, 2362-2367, 1978.

17 Bond, G., Broecker, W., Johnsen, S., McManus, J., Labeyrie, L., Jouzel, J., and Bonani, G.:
18 Correlations between climate records from North Atlantic sediments and Greenland ice,
19 *Nature*, 365, 143–147, 1993.

20 Broecker, W. S.: Massive iceberg discharges as triggers for global climate change, *Nature*,
21 372, 421–424, 1994.

22 Cai, Y., Fung, I. Y., Edwards, R. L., An, Z., Cheng, H., Lee, J. E., Tan, L., Shen, C. C., Wang,
23 X., Day, J. A., Zhou, W. J., Kelly, M. J., and Chiang, J. C. H.: Variability of
24 stalagmite-inferred Indian monsoon precipitation over the past 252,000 y, *Proc. Natl. Acad.
25 Sci. U. S. A.*, 112, 2954-2959, 2015.

26 Caley, T., Roche, D. M., and Renssen, H.: Orbital Asian summer monsoon dynamics
27 revealed using an isotope-enabled global climate mode, *Nat. Commun.*, 5,

1 doi:10.1038/ncomms6371, 2014.

2 Channell, J. E. T., Hodell, D. A., Romero, O., hillaire-Marcel, C., Vernal, A. D., Stoner, J. S.,
3 Mazaud, A., and Röhl, U.: A 750-kyr detrital-layer stratigraphy for the North Atlantic (IODP
4 Sites U1302–U1303, Orphan Knoll, Labrador Sea), *Earth Planet. Sc. Lett.*, 317–318,
5 218–230, 2012.

6 Chen, F., Bloemendal, J., Wang, J., Li, J., and Oldfield, F.: High-resolution multi-proxy
7 climate records from Chinese loess: evidence for rapid climatic changes over the last 75 kyr,
8 *Palaeogeogr. Palaeoclimatol.*, 130, 323–335, 1997.

9 Chen, J., Chen, Y., Liu, L., Ji, J., Balsam, W., Sun, Y., and Lu, H.: Zr/Rb ratio in the Chinese
10 loess sequences and its implication for changes in the East Asian winter monsoon strength,
11 *Geochim. Cosmochim. Acta.*, 70, 1471–1482, 2006.

12 Cheng, H., Edwards, R. L., Broecker, W. S., Denton, G. H., Kong, X., Wang, Y., Zhang, R.,
13 and Wang, X.: Ice age terminations, *Science*, 326, 248–252, 2009.

14 Cheng, H., Edwards, R. L., Kong, X., Ming, Y., Kelly, M. J., Wang, X., Gallup, C. D., and
15 Liu, W.: A penultimate glacial monsoon record from Hulu Cave and two-phase glacial
16 terminations, *Geology*, 34, 217–220, 2006.

17 Cheng, H., Zhang, P., Spötl, C., Edwards, R. L., Cai, Y., Zhang, D., and Sang, W.: The
18 climate cyclicality in semiarid-arid central Asia over the past 500,000 years, *Geophys. Res.*
19 *Lett.*, 39, L01705, doi:10.1029/2011GL050202, 2012.

20 Clark, P. U., Alley, R. B., and Pollard, D.: Northern Hemisphere ice-sheet influences on
21 global climate change, *Science*, 286, 1104–1111, 1999.

22 Clemens, S. C., Prell, W. L., and Sun, Y.: Orbital-scale timing and mechanisms driving Late
23 Pleistocene Indo-Asian summer monsoons: reinterpreting cave speleothem $\delta^{18}\text{O}$,
24 *Paleoceanography*, PA4207, doi:10.1029/2010PA001926, 2010.

25 Dansgaard, W., Johnsen, S. J., Clausen, H. B., Dahl-Jensen, D., Gundestrup, N. S., Hammer,
26 C. U., Hvidberg, C. S., Steensen, J. P., Sveinbjornsdottir, A. E., Jouzel, J., and Bond, G.:
27 Evidence for general instability of past climate from a 250-kyr ice-core record, *Nature*, 364,

1 218–220, 1993.

2 Dayem, K. E., Molnar, P., Battisti, D. S., and Roe, G. H.: Lessons learned from oxygen
3 isotopes in modern precipitation applied to interpretation of speleothem records of
4 paleoclimate from eastern Asia, *Earth Planet. Sc. Lett.*, 295, 219–230, 2010.

5 Ding, Z., Derbyshire, E., Yang, S., Yu, Z., Xiong, S., and Liu, T.: Stacked 2.6-Ma grain size
6 record from the Chinese loess based on five sections and correlation with the deep-sea $\delta^{18}\text{O}$
7 record, *Paleoceanography*, 17, 5-1-5-21, 2002.

8 Ding, Z., Liu, T., Rutter, N. W., Yu, Z., Guo, Z., and Zhu, R.: Ice-Volume forcing of East
9 Asian winter monsoon variations in the past 800,000 years, *Quaternary Res.*, 44, 149–159,
10 1995.

11 Ding, Z., Ren, J., Yang, S., and Liu, T.: Climate instability during the penultimate glaciation:
12 evidence from two high-resolution loess records, China, *J. Geophys. Res.*, 104, 20123–20132,
13 1999.

14 Ding, Z., Rutter, N. W., Liu, T., Ren, J., Sun, J., and Xiong, S.: Correlation of Dansgaard–
15 Oeschger cycles between Greenland ice and Chinese loess, *Paleoclimates*, 4, 281–291, 1998.

16 Ding, Z., Yu, Z., Rutter, N. W., and Liu, T.: Towards an orbital time scale for Chinese loess
17 deposits, *Quaternary Sci. Rev.*, 13, 39–70, 1994.

18 Fang, X., Pan, B., Guan, D., Li, J., Yugo, O., Hitoshi, F., and Keiichi, O.: A 60000-year
19 loess-paleosol record of millennial-scale summer monsoon instability from Lanzhou, China,
20 *Chinese Sci. Bull.*, 44, 2264–2267, 1999.

21 Gao, Y.: On some problems of Asian monsoon, in: *Some Questions About the East Asian*
22 *Monsoon*, edited by: Gao, Y., Science Press, Beijing, 1–49, 1962.

23 Garidel-Thoron, T. D., Beaufort, L., Linsley, B. K., and Dannenmann, S.: Millennial-scale
24 dynamics of the East Asian winter monsoon during the last 200,000 years, *Paleoceanography*,
25 16, 491–502, 2001.

26 Gloersen, P. and Huang, N.: Comparison of interannual intrinsic modes in hemispheric ice
27 covers and other geophysical parameters, *IEEE Transactions in Geosciences and Remote*

1 Sensing, 41, 1062-1074, 2003.

2 Guo, Z., Liu, T., Guiot, J., Wu, N., Lv, H., Han, J., Liu, J., and Gu, Z.: High frequency pulses
3 of East Asian monsoon climate in the last two glaciations: link with the North Atlantic, *Clim.*
4 *Dynam.*, 12, 701–709, 1996.

5 Halley, E.: An historical account of the trade winds and monsoons observable in the seas
6 between and near the tropics with an attempt to assign the physical cause of the said wind,
7 *Philos. T. R. Soc. Lond.*, 16, 153–168, 1986.

8 Heinrich, H.: Origin and consequences of cyclic ice rafting in the Northeast Atlantic Ocean
9 during the past 130,000 years, *Quaternary Res.*, 29, 142–152, 1988.

10 Hu, C., Henderson, G. M., Huang, J., Xie, S., Sun, Y., and Johnson, K. R.: Quantification of
11 Holocene Asian monsoon rainfall from spatially separated cave records, *Earth Planet. Sc.*
12 *Lett.*, 266, 221–232, 2008.

13 Hu, Z. and Wu, Z.: The intensification and shift of the annual North Atlantic Oscillation in a
14 global warming scenario simulation, *Tellus*, 56, 112-124, 2004.

15 Huang, N. E., Shen, Z., Long, S. R., Wu, M. C., Shih, H. H., Zheng, Q., Yen, N. C., Tung, C.
16 C., and Liu, H. H.: The empirical mode decomposition and the Hilbert spectrum for nonlinear
17 and non-stationary time series analysis, *The Royal Society*, 454, 903-995, 1998.

18 Jin, L., Chen, F., Ganopolski, A., and Claussen, M.: Response of East Asian climate to
19 Dansgaard/Oeschger and Heinrich events in a coupled model of intermediate complexity, *J.*
20 *Geophys. Res.*, 112, D06117, doi:10.1029/2006JD007316, 2007.

21 Kelly, M. J., Edwards, R. L., Cheng, H., Yuan, D., Cai, Y., Zhang, M., Lin, Y., and An, Z.:
22 High resolution characterization of the Asian Monsoon between 146,000 and 99,000 years B.
23 P. from Dongge Cave and global correlation of events surrounding Termination II,
24 *Palaeogeogr. Palaeocl.*, 236, 20–38, 2006.

25 Lestari, R. and Iwasaki, T.: A GCM study on the roles of the seasonal marches of the SST
26 and land–sea thermal contrast in the onset of the Asian summer monsoon, *J. Meteorol. Soc.*
27 *Jpn.*, 84, 69–83, 2006.

- 1 Lin, Z. and Wang, S.: EMD analysis of solar insolation, *Meteorol. Atmos. Phys.*, 93, 123-128,
2 2006.
- 3 Lisiecki, L. E. and Raymo, M. E.: A Pliocene-Pleistocene stack of 57 globally distributed
4 benthic $\delta^{18}\text{O}$ records, *Paleoceanography*, 20, PA1003, doi:10.1029/2004PA001071, 2005.
- 5 Liu, T. and Ding, Z.: Chinese loess and the paleomonsoon, *Annu. Rev. Earth Pl. Sc.*, 26,
6 111–145, 1998.
- 7 Liu, T., Ding, Z., and Rutter, N.: Comparison of Milankovitch periods between continental
8 loess and deep sea records over the last 2.5 Ma, *Quaternary Sci. Rev.*, 18, 1205–1212, 1999.
- 9 Liu, Z., Wen, X., Brady, E. C., Otto-Bliesner, B., Yu, G., Lu, H., Cheng, H., Wang, Y.,
10 Zheng, W., Ding, Y., Edwards, R. L., Cheng, J., Liu, W., and Yang, H.: Chinese cave records
11 and the East Asian Summer Monsoon, *Quaternary Sci. Rev.*, 83, 115-128, 2014.
- 12 Lu, H., Huissteden, K. V., An, Z., Nugteren, G., and Vandenberghe, J.: East Asia winter
13 monsoon variations on a millennial time-scale before the last glacial–interglacial cycle, *J.*
14 *Quaternary Sci.*, 14, 101–110, 1999.
- 15 Lu, H., Yi, S., Liu, Z., Mason, J. A., Jiang, D., Cheng, J., Stevens, T., Xu, Z., Zhang, E., Jin,
16 L., Zhang, Z., Guo, Z., Wang, Y., and Otto-Bliesner, B.: Variation of East Asian monsoon
17 precipitation during the past 21 k.y., and potential CO_2 forcing, *Geology*, 41, 1023–1026,
18 2013.
- 19 Lu, H., Zhang, F., and Liu, X.: Patterns and frequencies of the East Asian winter monsoon
20 variations during the past million years revealed by wavelet and spectral analyses, *Global*
21 *Planet. Change*, 35, 67–74, 2003.
- 22 Maher, B. A. and Thompson, R.: Oxygen isotopes from Chinese caves: records not of
23 monsoon rainfall but of circulation regime, *J. Quaternary Sci.*, 27, 615–624, 2012.
- 24 McManus, J. F., Oppo, D. W., and Cullen, J. L.: A 0.5-million-year record of millennial-scale
25 climate variability in the North Atlantic, *Science*, 283, 971–975, 1999.
- 26 Meese, D. A., Gow, A. J., Alley, R. B., Zielinski, G. A., Grootes, P. M., Ram, M., Taylor, K.
27 C., Mayewski, P. A., and Blozan, J. F.: The Greenland Ice Sheet Project 2 depth-age scale:

1 methods and results, *J. Geophys. Res.*, 102, 26411–26423, 1997.

2 Miao, X., Sun, Y., Lu, H., and Mason, J. A.: Spatial pattern of grain size in the Late Pliocene
3 “Red Clay” deposits (North China) indicates transport by low-level northerly winds,
4 *Palaeogeogr. Palaeoclimatol.*, 206, 149–155, 2004.

5 Molla, K., Sumi, A., and Rahman, M.: Analysis of temperature change under global warming
6 impact using Empirical Mode Decomposition, *Int. J. Information Technol.*, 3, 131-139, 2006.

7 Palmer, T. N. and Sun, Z.: A modelling and observational study of the relationship between
8 sea surface temperature in the North-West Atlantic and the atmospheric general circulation,
9 *Q. J. Roy. Meteor. Soc.*, 111, 947–975, 1985.

10 Pausata, F. S. R., Battisti, D. S., Nisancioglu, K. H., and Bitz, C. M.: Chinese stalagmite $\delta^{18}\text{O}$
11 controlled by changes in the Indian monsoon during a simulated Heinrich event, *Nat. Geosci.*,
12 4, 474–480, 2011.

13 Peterse, F., Prins, M. A., Beets, C. J., Troelstra, S. R., Zheng, H., Gu, Z., Schouten, S., and
14 Damsté, J. S. S.: Decoupled warming and monsoon precipitation in East Asia over the last
15 deglaciation, *Earth Planet. Sc. Lett.*, 301, 256–264, 2011.

16 Porter, S. C. and An, Z.: Correlation between climate events in the North Atlantic and China
17 during the last glaciation, *Nature*, 375, 305–308, 1995.

18 Rodwell, M. J., Rowell, D. P., and Folland, C. K.: Oceanic forcing of the wintertime North
19 Atlantic Oscillation and European climate, *Nature*, 398, 320–323, 1999.

20 Schulz, M. and Mudelsee, M.: REDFIT: estimating red-noise spectra directly from unevenly
21 spaced paleoclimatic time series, *Comput. Geosci.*, 28, 421–426, 2002.

22 Schulz, M. and Stahler, K.: Spectrum: spectral analysis of unevenly spaced palaeoclimatic
23 time series, *Comput. Geosci.*, 23, 929-945, 1997.

24 Shi, Z., Liu, X., Sun, Y., An, Z., Liu, Z., and Kutzbach, J.: Distinct responses of East Asian
25 summer and winter monsoons to astronomical forcing, *Clim. Past*, 7, 1363–1370, 2011.

26 Sun, Y., Clemens, S. C., An, Z., and Yu, Z.: Astronomical timescale and palaeoclimatic
27 implication of stacked 3.6-Myr monsoon records from the Chinese Loess Plateau, *Quaternary*

1 Sci. Rev., 25, 33–48, 2006.

2 Sun, Y., Clemens, S. C., Morrill, C., Lin, X., Wang, X., and An, Z.: Influence of Atlantic
3 meridional overturning circulation on the East Asian winter monsoon, *Nat. Geosci.*, 5, 46–49,
4 2012.

5 Sun, Y., Kutzbach, J., An, Z., Clemens, S., Liu, Z., Liu, W., Liu, X., Shi, Z., Zheng, W.,
6 Liang, L., Yan, Y., and Li, Y.: Astronomical and glacial forcing of East Asian summer
7 monsoon variability, *Quaternary Sci. Rev.*, 115, 132-142, 2015.

8 Sun, Y., Wang, X., Liu, Q., and Clemens, S. C.: Impacts of post-depositional processes on
9 rapid monsoon signals recorded by the last glacial loess deposits of northern China, *Earth
10 Planet. Sc. Lett.*, 289, 171–179, 2010.

11 Vautard, R., Yiou, P., and Ghil, M.: Singular-spectrum analysis: a toolkit for short, noisy
12 chaotic signals, *Physica D: Nonlinear Phenomena*, 58, 95-126, 1992.

13 Wang, L., Sarnthein, M., Erlenkeuser, H., Grimalt, J., Grootes, P., Heilig, S., Ivanova, E.,
14 Kienast, M., Pelejero, C., Pflaumaan, U.: East Asian monsoon climate during the Late
15 Pleistocene: high-resolution sediment records from the South China Sea, *Mar. Geol.*, 156,
16 245–284, 1999.

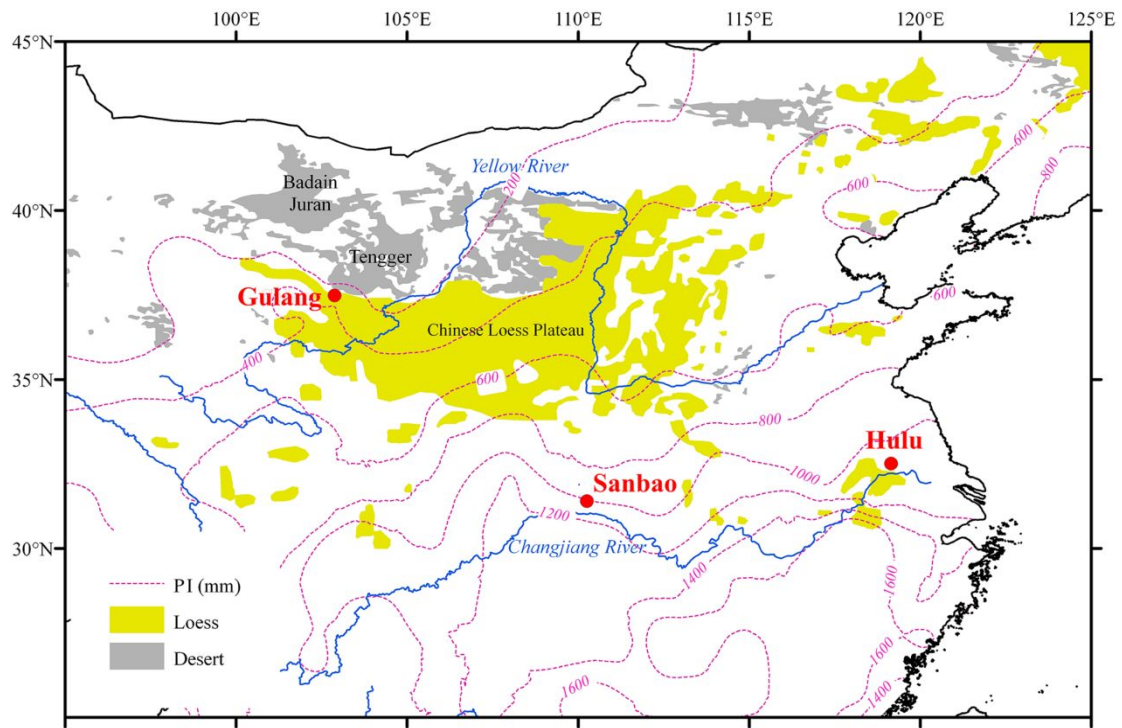
17 Wang, P., Clemens, S., Beaufort, L., Braconnot, P., Ganssen, G., Jian, Z., Kershaw, P.,
18 Sarnthein, M.: Evolution and variability of the Asian monsoon system: state of the art and
19 outstanding issues, *Quaternary Sci. Rev.*, 24, 595-629, 2005.

20 Wang, Y., Cheng, H., Edwards, R. L., An, Z., Wu, J., Shen, C., and Dorale, J. A.: A high
21 resolution absolute-dated late Pleistocene monsoon record from Hulu Cave, China, *Science*,
22 294, 2345–2348, 2001.

23 Wang, Y., Cheng, H., Edwards, R.L., Kong, X., Shao, X., Chen, S., Wu, J., Jiang, X., Wang,
24 X., and An, Z.: Millennial and orbital-scale changes in the East Asian monsoon over the past
25 224,000 years, *Nature*, 451, 1090–1093, 2008.

26 Xiao, J., Porter, S. C., An, Z., Kumai, H., and Yoshikawa, S.: Grain size of quartz as an
27 indicator of winter monsoon strength on the Loess Plateau of central China during the last

- 1 130,000 yr, *Quaternary Res.*, 43, 22–29, 1995.
- 2 Yang, S. and Ding, Z.: A 249 kyr stack of eight loess grain size records from northern China
3 documenting millennial-scale climate variability, *Geochem. Geophys. Geosy.*, 15, 798–814,
4 2014.
- 5 Yang, Z., Lin, Z., and Yu, M.: Multi-scale analysis of East Asian winter monsoon evolution
6 and Asian inland drying force (in Chinese), *Quaternary Sci.*, 31, 73–80, 2011.
- 7 Yang, Z., Lin, Z., Yu, M., Zhang, Z.: Significant multi-scale analysis on evolution of the East
8 Asian summer monsoon on the Loess Plateau during the last 1 MaB.P. (in Chinese),
9 *Geography and Geo-information Science*, 24, 93-97, 2008.
- 10 Yuan, D., Cheng, H., Edwards, R. L., Dykoski, C. A., Kelly, M. J., Zhang, M., Qing, J., Lin,
11 Y., Wang, Y., Wu, J., Dorale, J. A., An, Z., and Cai, Y.: Timing, duration, and transitions of
12 the last interglacial Asian monsoon, *Science*, 304, 575–578, 2004.
- 13 Zhang, R. and Delworth, T. L.: Simulated tropical response to a substantial weakening of the
14 Atlantic thermohaline circulation, *J. Climate*, 18, 1853–1860, 2005.
- 15

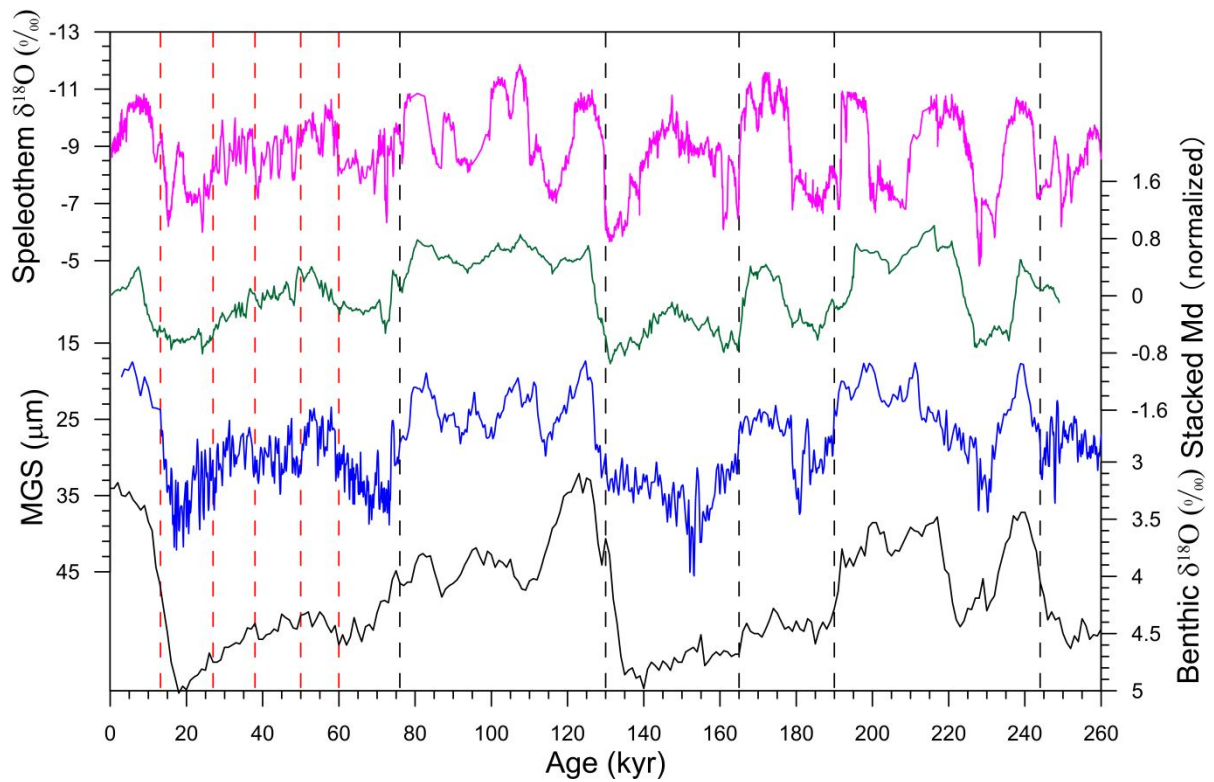


1

2 Figure 1. Map showing the loess distribution and locations of Gulang loess section, Sanbao,
 3 and Hulu caves. Dotted lines indicate the precipitation isohyets (PI).

4

1

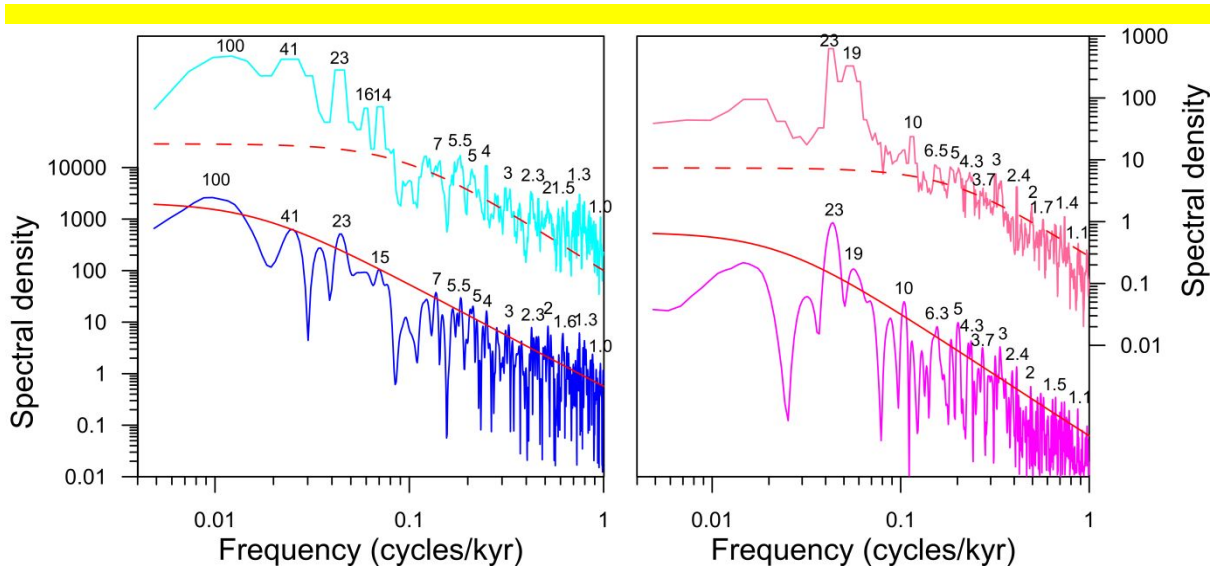


2

3 Figure 2. Comparison of Gulang MGS (blue, Sun et al., 2015) and CHILOMOS stack Median
4 grain size (Md, green, Yang and Ding, 2014) with the benthic $\delta^{18}\text{O}$ (black, Lisiecki and
5 Raymo, 2005) and Sanbao/Hulu speleothem $\delta^{18}\text{O}$ (magenta, Wang et al., 2008; Cheng et al.,
6 2009) records. The red and black dashed lines denote tie points derived from optically
7 stimulated luminescence (OSL) dating and benthic $\delta^{18}\text{O}$ correlation, respectively.

8

1



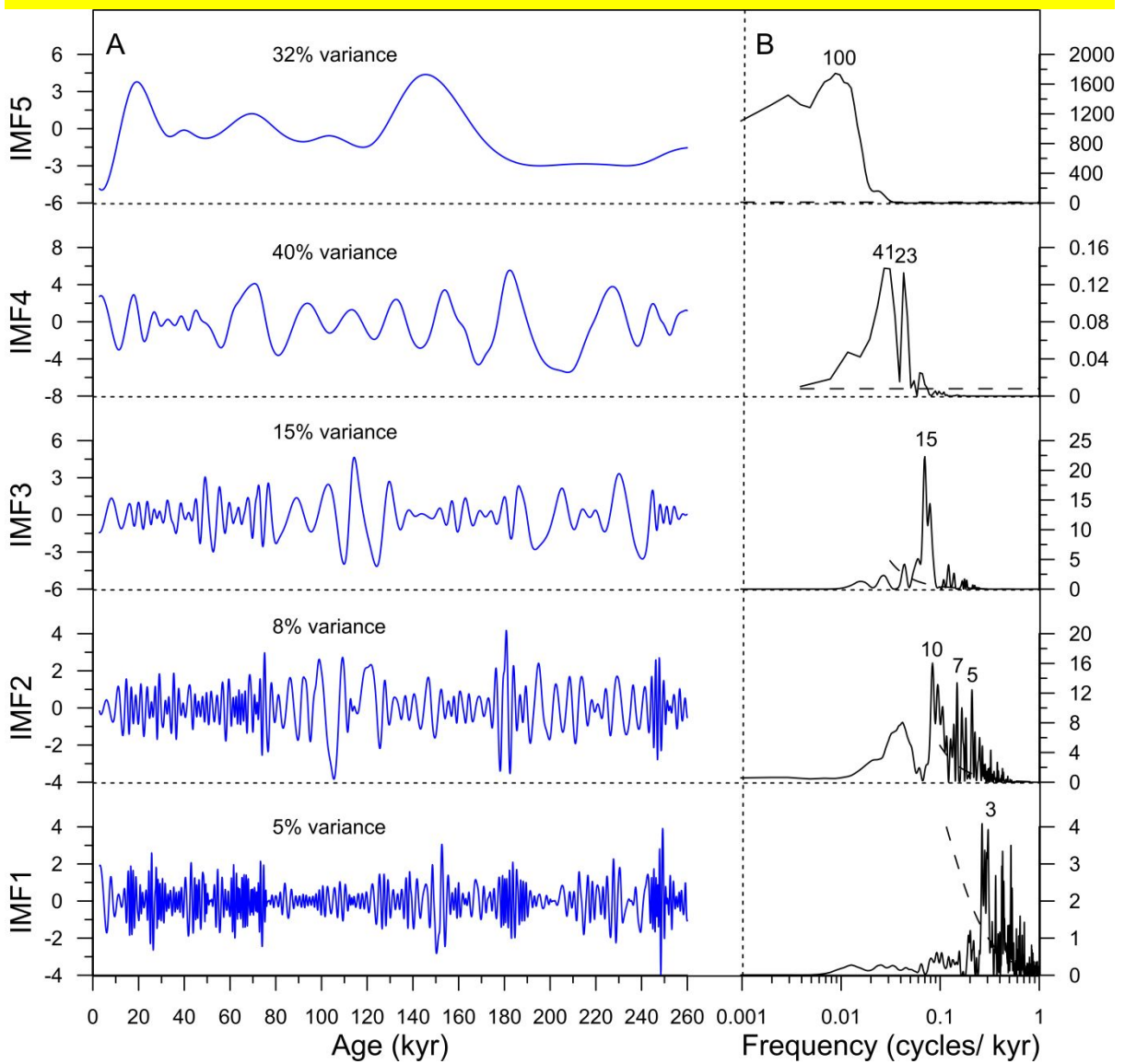
2

3 Figure 3. Spectrum results of Gulang MGS (A) and Sanbao/Hulu speleothem $\delta^{18}\text{O}$ (B) (Wang
4 et al., 2008; Cheng et al., 2009) records using REDFIT (lower) and MTM (higher) methods.

5 The red lines represent the 80% (solid) and 90% (dotted) confidence levels. Periodicities are
6 shown above the spectral curves.

7

1



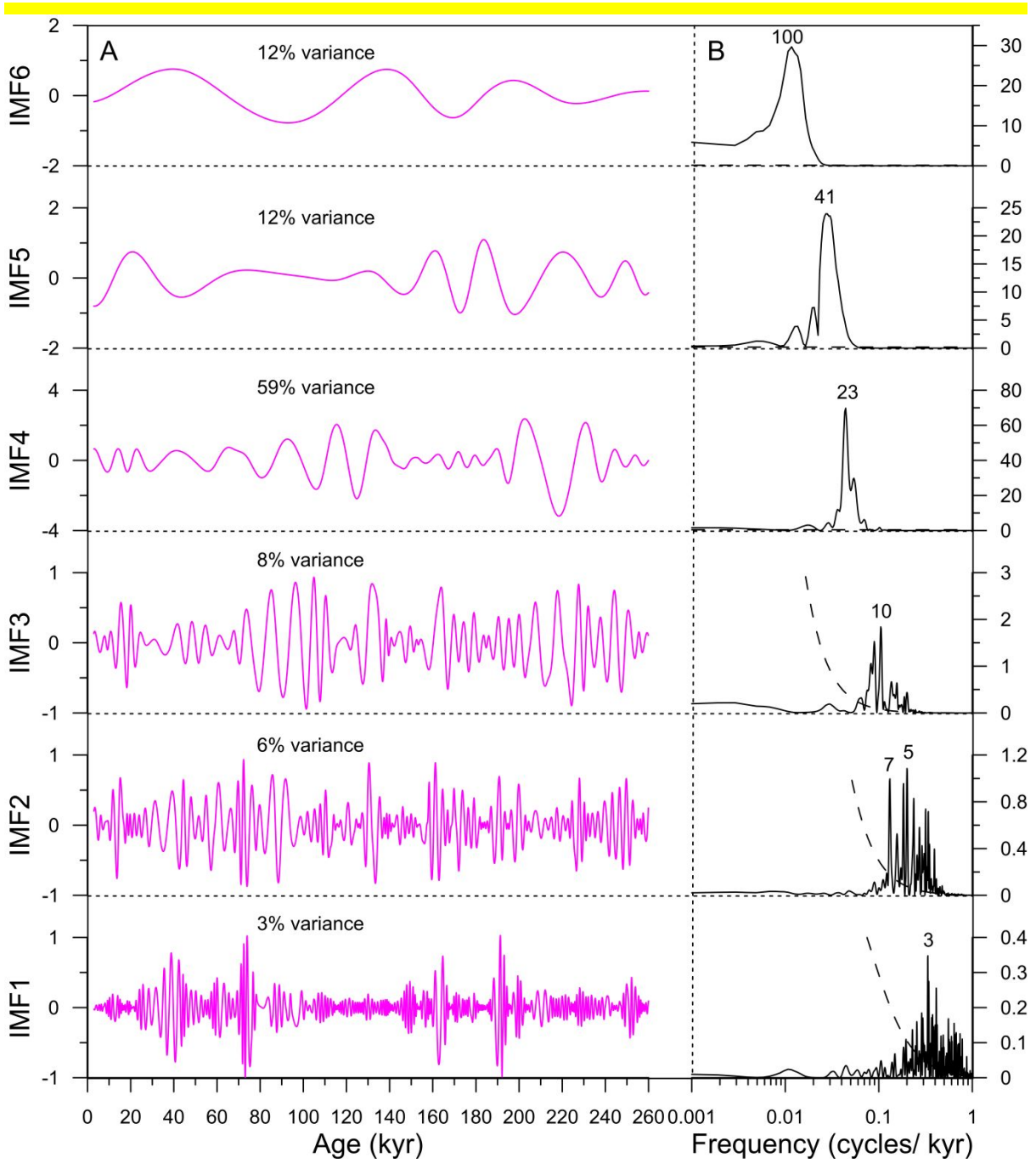
2

3 Figure 4. IMFs of Gulang MGS series (A) and corresponding spectrum (B). Black numbers

4 are dominant periods and dotted lines represent the 90% confidence level.

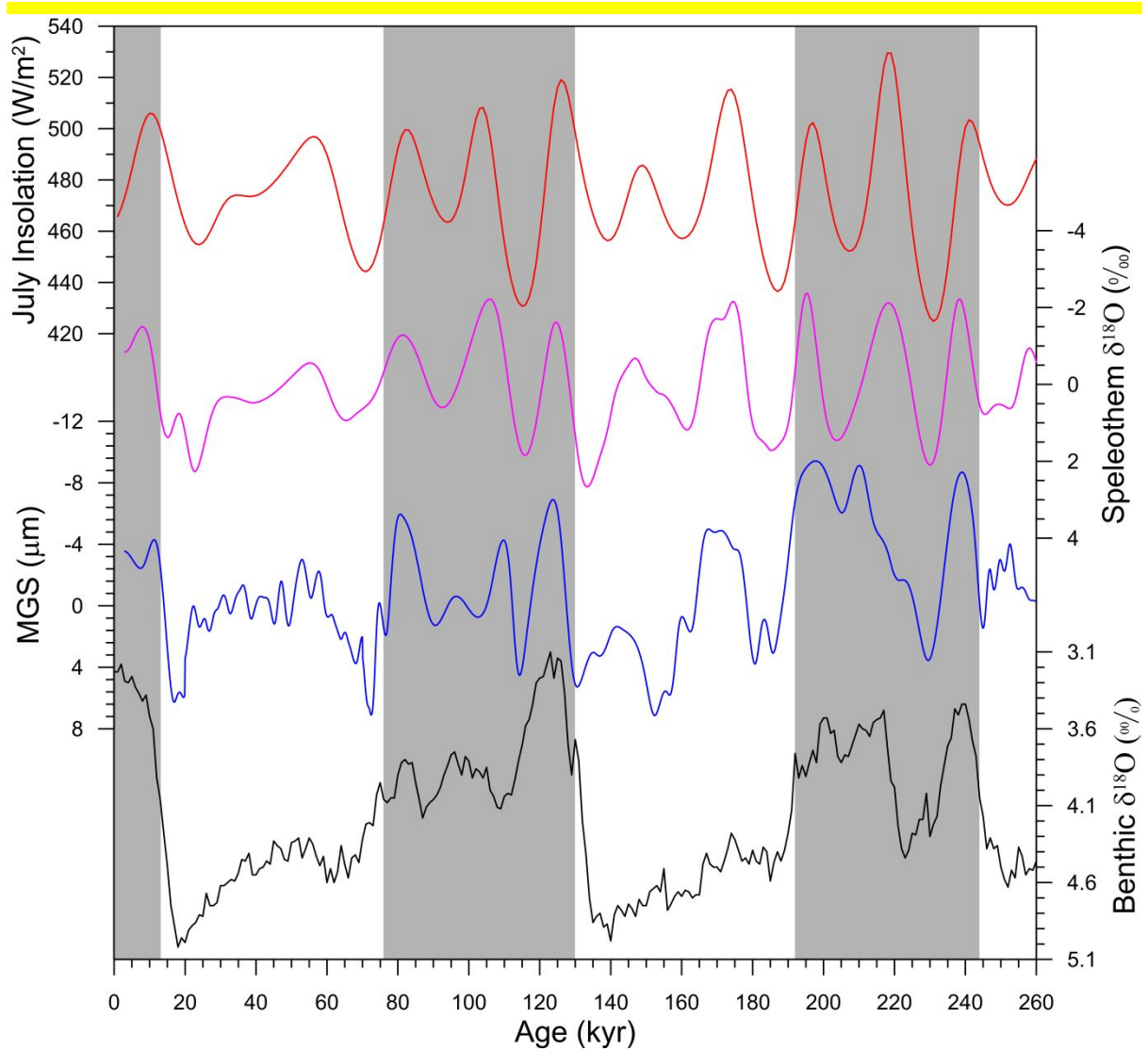
5

1



2

3 Figure 5. IMFs of speleothem $\delta^{18}\text{O}$ series (A) and corresponding spectrum (B). Black
4 numbers are dominant periods and dotted lines represent the 90% confidence level.

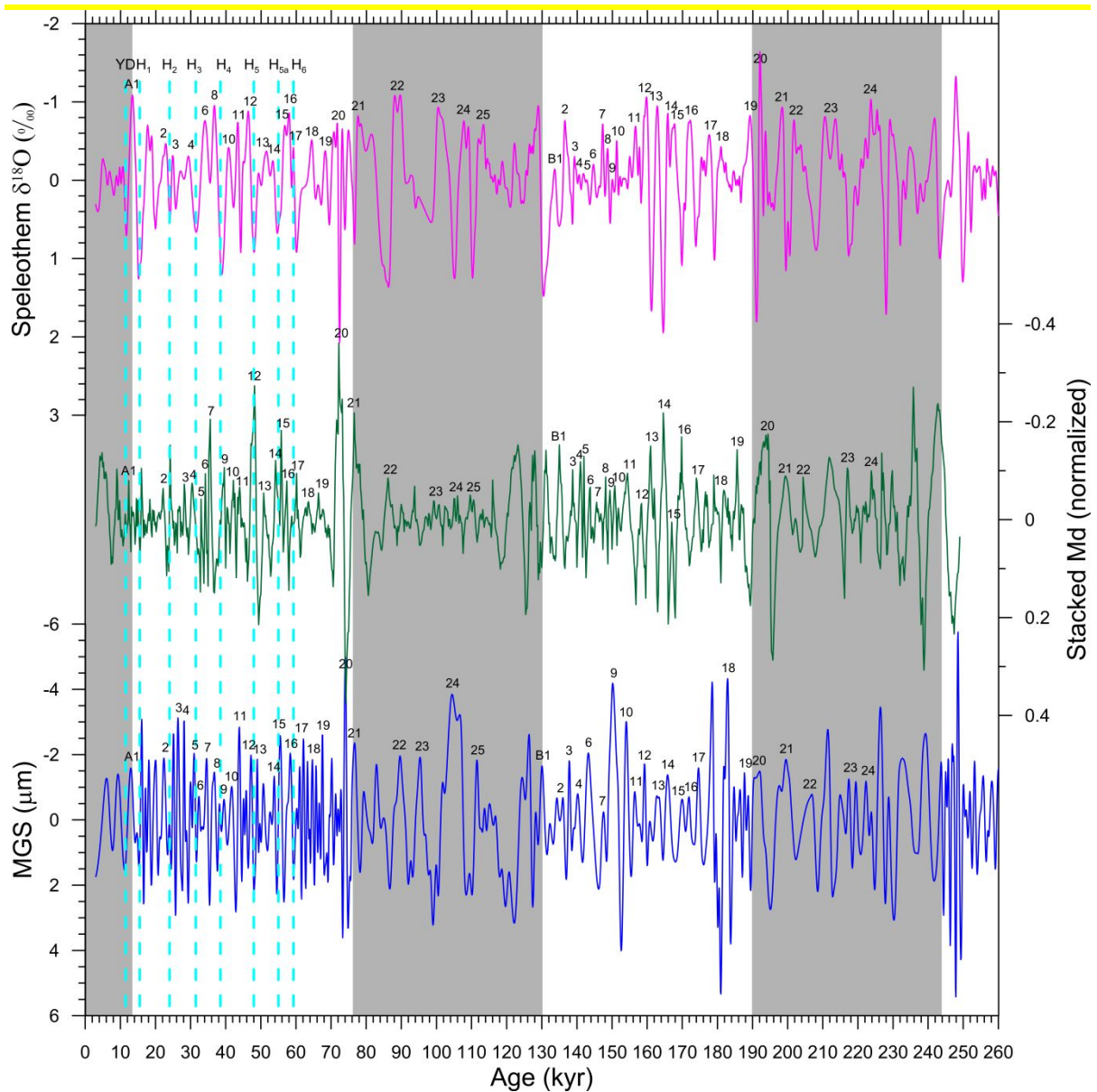


1

2 Figure 6. Comparison of the glacial-and-orbital scale components of Gulang MGS (blue) and
 3 Sanbao/Hulu speleothem $\delta^{18}\text{O}$ (magenta, Wang et al., 2008; Cheng et al., 2009) records with
 4 summer insolation at 65°N (red, Berger, 1978) and benthic $\delta^{18}\text{O}$ record (black, Lisiecki and
 5 Raymo, 2005). The vertical gray bars represent the interglacial periods.

6

1



2

3 Figure 7. Comparison of millennial-scale variations among Gulang MGS (blue), CHILOMOS
 4 stack Md (green, [Yang and Ding, 2014](#)) and Sanbao/Hulu speleothem $\delta^{18}O$ (magenta, [Wang](#)
 5 [et al., 2008](#); [Cheng et al., 2009](#)) records over the last two glacial–interglacial cycles. Cyan
 6 dotted lines are the YD and the Heinrich events **identified among** the three records and gray
 7 bars indicate interglacial periods. The numbers represent well-correlated Chinese interstadials
 8 identified among the three records.